Engebretson Mark, J. (Orcid ID: 0000-0002-3882-8108)
Pilipenko Vyacheslav (Orcid ID: 0000-0003-3056-7465)
Moldwin Mark, B. (Orcid ID: 0000-0003-0954-1770)
Connors Martin (Orcid ID: 0000-0003-0634-9599)
Weygand James, M. (Orcid ID: 0000-0001-7996-2277)
Mann Ian (Orcid ID: 0000-0003-1004-7841)
Russell Christopher, T. (Orcid ID: 0000-0003-1639-8298)
Vorobev Andrei, V. (Orcid ID: 0000-0002-9680-5609)

Nighttime Magnetic Perturbation Events Observed in Arctic Canada, 1, Survey and Statistical Analysis

M. J. Engebretson[1], V. A. Pilipenko[1,2], L. Y. Ahmed[1], J. L. Posch[1], E. S. Steinmetz[1], M. B. Moldwin[3], M. G. Connors[4], J. M. Weygand[5], I. R. Mann[6], D. H. Boteler[7], C. T. Russell[8], and A.V. Vorobev[9]

[1]Augsburg University, Minneapolis, MN

[2]Institute of Physics of the Earth, Moscow, Russia

[3]University of Michigan, Ann Arbor, MI

[4]Athabasca University, Athabasca, AB

[5]IGPP/UCLA---ESS, Los Angeles, CA

[6]University of Alberta, Edmonton, AB, Canada

[7]Natural Resources Canada, Ottawa, ON, Canada

[8]University of California, Los Angeles, Earth Planetary and Space Sciences, Los Angeles, CA

[9]Ufa State Aviation Technical University, Ufa, Russia

This is the author manuscript accepted for publication and has undergone full peer review but has not been through the copyediting, typesetting, pagination and proofreading process, which may lead to differences between this version and the Version of Record. Please cite this article as doi: 10.1029/2019JA026794

revised version to be submitted to the Journal of Geophysical Research – Space Physics
version of May 22, 2019

Key Words: magnetic impulse events, substorms, magnetic storms, geomagnetically-induced currents

Key Points:

- Most intense events were associated with substorms; their association with magnetic storms was much lower above 73° MLAT.
- Largest |dB/dt| values appeared within a ~275 km radius associated with a region of shear between upward and downward field-aligned currents.
- The statistical distributions of impulse amplitudes of both |ΔX| and |dX/dt| fit well the log-normal distribution, but varied with latitude.

Abstract

The rapid changes of magnetic fields associated with large, isolated magnetic perturbations with amplitudes |ΔB| of hundreds of nTs and 5-10 min periods can induce bursts of geomagnetically-induced currents that can harm technological systems. This paper presents statistical summaries of the characteristics of nightside magnetic perturbation events observed in Eastern Arctic Canada from 2014 through 2017 using data from stations that are part of four magnetometer arrays: MACCS, AUTUMNX, CANMOS, and CARISMA, covering a range of magnetic latitudes from 68° to 78°. Most but not all of the magnetic perturbation events were associated with substorms: roughly 2/3 occurred between 5 and 30 minutes after onset. The association of intense nighttime magnetic perturbation events with magnetic storms was significantly reduced at latitudes above 73°, presumably above the nominal auroral oval. A superposed epoch study of 21 strong events at Cape Dorset showed that the largest |dB/dt| values appeared within a ~275 km radius that was associated with a region of shear between upward and downward field-aligned currents. The statistical distributions of impulse amplitudes of both |ΔB| and |dB/dt| fit well the log-normal distribution at all stations. The |ΔB| distributions are similar over the magnetic latitude range studied, but the kurtosis and skewness of the |dB/dt| distributions show a slight increase with latitude. Knowledge of the statistical characteristics of these events has enabled us to estimate the occurrence probability of extreme impulsive disturbances using the approximation of a log-normal distribution.

1. Introduction

Space weather caused by the interaction of solar ejecta with the near-Earth environment activates global electromagnetic and plasma processes: intensification of the magnetosphere - ionosphere current systems, energization of ring current and radiation belt particles, bursts of precipitation into the auroral oval, etc. One of the most significant factors of space weather for terrestrial technological systems is electric geomagnetically induced currents (GICs) related to abrupt changes of the geomagnetic field dB/dt (e.g., *Boteler et al.,* 1998; *Lanzerotti,* 2001; *Kappenman,* 2005; *Knipp,* 2015). Therefore, significant efforts and resources of the geophysical community are aimed at global MHD modeling of storm/substorm activity augmented by the magnetotelluric reconstruction of telluric currents (*Pulkkinen et al.*, 2007; *Zhang et al.*, 2012). However, the highest risk of GIC may be related not directly to those processes with enormous energy yield, but to more localized and rapid processes. Though the power of such processes is many orders of magnitude lower than the power of magnetospheric storms and substorms, the rapidly varying electromagnetic fields of these events can induce a significant GIC (*Viljanen*, 1997; *Viljanen et al.*, 1998).

The interaction between the solar wind and the magnetosphere serves as a source of diverse types of nonstationary processes and perturbations of different spatial and temporal scales. As a result, intense disturbances can be observed not only during periods of high magnetospheric activity (magnetic storms and substorms), but also under quiet geomagnetic conditions. Such impulsive perturbations are now understood to include sudden impulses/sudden commencements (SIs/SCs) and traveling convection vortices (TCVs), which are a response to a local impact on the magnetosphere and are specific for the daytime high-latitude ionosphere (*Friis-Christensen et al.,* 1988; *Engebretson et al.,* 2013). The terrestrial manifestation of a TCV at a single station is an isolated magnetic impulse event (MIE) – a sporadic perturbation of the geomagnetic field with a duration of ~5-10 min and with amplitude of ~100 nT (*Lanzerotti et al.,* 1990; *Vorobjev et al.,* 1993).

In addition to dayside TCVs, intense magnetic perturbation events - large, isolated pulses with similar periods - often appear in ground-based magnetometer records during nighttime. Case studies of these intense nighttime events, augmented by observations from auroral imagers and high-altitude spacecraft in the nightside magnetosphere, can be found in a companion paper (*Engebretson et al.,* 2019, hereafter called Paper 2).

Nighttime magnetic perturbation events observed at auroral zone latitudes have often been associated with magnetic storms and/or substorms, but the occurrence rate and characteristics of these events in the high latitude regions that are the focus of this study are still relatively unknown.

This paper presents a statistical survey of nighttime magnetic perturbation events recorded by stations in Arctic Canada. Section 2 introduces the data set and outlines the event identification technique. Section 3 presents a statistical survey of intense events recorded during 2015 by selected stations in the MACCS, AUTUMNX, CANMOS, and CARISMA magnetometer arrays, and section 4 presents a study of their occurrence as a function of the phase of magnetic storms. Section 5 presents data from one high latitude MACCS station (Repulse Bay) during 2015 and 2017 in order to examine the temporal association between these events and both substorms and magnetic storms. Section 6 presents a superposed epoch analysis of nighttime events observed at MACCS station Cape Dorset from mid-2014 through 2016, and section 7 presents analyses of the probability distribution functions of these events at selected stations during 2015 and 2017. Section 8 discusses the observations in the light of other recent studies, and section 9 presents a summary.

2. Data Set and Event Identification Technique

Eastern Arctic Canada is the only region providing dense two-dimensional ground magnetometer coverage at latitudes from the central auroral zone through contracted oval latitudes and into the near-cusp and polar cap regions. This paper presents statistical summaries of the characteristics of nighttime magnetic perturbation events observed in this region from 2014 through 2017 using data from stations that are part of four magnetometer arrays: MACCS (Engebretson et al., 1995), AUTUMNX (Connors et al., 2016), CANMOS (Nikitina et al., 2016) and CARISMA (Mann et al., 2008). Locations of the 8 magnetometers used in this study are shown in Figure 1, and Table 1 lists their geographic and corrected geomagnetic coordinates and data sampling rates. Magnetic field variations are in local geomagnetic coordinates X (North-South), Y(East-West), and Z (vertical).

Magnetic perturbation events included in this study were selected using the following procedure, which combined visual identification of impulsive events with automated capture of the extreme values of both the magnetic field values and their time derivatives: Each day's daily magnetogram (daily 3-axis

plot) was first displayed on a computer screen. In nearly all cases the X component perturbation was negative, but the Y and Z perturbations could be either unipolar or bipolar.

Figure 2 shows three examples of portions of such daily magnetograms that each include an isolated nighttime event. Each of the three events shown in this figure was preceded by a steady magnetic field during most of the hour prior to onset. All three components of the event shown in Figure 2b demonstrate a single strong negative spike near 0130 UT with duration <10 min but weaker continuing activity for nearly 4 hours after the large magnetic perturbation. The X component in Figure 2b returned to nearly its original level after ~10 min, while the Y component included a negative bay of >1 h duration but also a short-duration negative pulse from 800 to 450 nT that returned to its original value in < 5 min. The negative pulse in the Z component also returned to its original value in < 5 min. Figures 2a and 2c both show isolated but more complex events. Each component in these figures included several 5-min duration spikes that were embedded within perturbations that returned only more gradually (from 30 min to 1 h) to their original levels. Note that Figures 2b and 2c show observations of the same event at two different locations. Both the fine structure and the larger context of nighttime events, as well as their amplitudes, often varied from station to station. Four examples of complex events observed at multiple stations are presented in Paper 2.

Once an event was identified, the IDL cursor function was used to visually select times before and after a region of interest containing an impulse. The data were subsequently displayed again covering only the selected times, and the cursor function was again used to select a narrower range of times beginning before the onset of the impulse and ending after the impulse (whether unipolar or bipolar) had returned to near the beginning value and before any subsequent impulse. A plot of this narrower range of times was produced and saved for further analysis, and the values of each component at the start of this second interval (the pre-onset values) were also saved. The range of values in each component in this time range was then automatically sorted and the extremal values and their occurrence times were recorded. The pre-onset values were then used as baselines to compare with the extremal values in order to derive the positive and negative excursion values for each component. Data in each component were then subjected to a 10 point smoothing to reduce noise and eliminate isolated bad data points, and numerically differentiated using the 3-point Lagrangian approximation, $dB/dt[i] = (B[i+1] - B[i-1]) / 2\Delta t$

(where Δt is the time step). We found that 10-point smoothing reduced the amplitude of single-point errors to levels far below those of the derivatives of large perturbation events, and reduced the peak values of derivatives by consistently much less than 5%. A plot of the time series of these derivatives was also produced and saved, and the maximum and minimum derivative values in this time range were automatically determined and recorded.

If a subsequent impulse was visually identified to have amplitude ≥200 nT in any component, this procedure was repeated to isolate it. In cases where two perturbation events occurred in close temporal proximity it was unclear what to select for beginning and end times. In such cases the accuracy of determining unipolar amplitude perturbations was reduced, but the accuracy of determining the maximum and minimum derivatives was not affected.

Figure 3 shows two scatter plots of amplitudes of events observed at Salluit in 2017 as a function of MLT. Figure 3a shows the peak to peak amplitudes of the X component, and Figure 3b shows the maximum (positive or negative) derivative of the X component. Similar figures were prepared for each component at each of the 8 stations during 2015 (not shown). Note, however, that the event selection threshold of ~200 nT in at least one component used in this study excludes many events in which no component's perturbation exceeded 200 nT. This figure and those from other stations do indicate, however, that large amplitude perturbation and derivative events occurring during nighttime hours greatly exceeded those occurring during daytime hours.

The technique described above was applied to all magnetic perturbation events, but in order to focus on nightside events and exclude those related to SIs, SSCs, and TCVs impinging on the dayside magnetopause, only events between 1600 and 0600 hours MLT were retained. Assuming a median UT of local noon at 17:30 hours (at the center of the array of selected stations), this MLT range is equivalent to a time range from 21:30 to 11:30 UT.

The largest nighttime events in 2015 were further checked for association with large solar wind pressure increases associated with SIs, SSCs, and the initial phases of magnetic storms by comparing event onsets with time-shifted IMF and solar wind data from the OMNI data base and the SYM/H index. OMNI data were not available for 3 days, but no SI events with $(\Delta Psw)/Psw > 1$ occurred within 1 hour prior to any of the nighttime events with $\Delta B > 1000$ nT or $dB/dt > 12$ nT/s recorded during the remaining

days at any of the 8 stations included in this study, and the SYM/H index for the 3 days with missing OMNI data showed no significant increase. OMNI and SYM/H data were also checked for all nighttime RBY and IGL events with $\Delta B > 600$ nT or $dB/dt > 6$ nT/s; only one SI event and two SSC events occurred within 1 hour prior to any of these MIEs.

It is well known that OMNI data from the L1 point cannot identify the presence of TCVs that originate in the ion foreshock. TCVs, however, usually have amplitudes well below 200 nT (Kataoka et al., 2003), so on the basis of our amplitude cutoff alone we also consider it unlikely that many (or any) TCVs are included in our much-larger-amplitude nighttime data sets.

As will be shown below, most of the nighttime impulse events we identified occurred from 5 min to 1 hour after substorm onset. During almost every nighttime event the IMF Bz component was negative, and in many cases it either exhibited large fluctuations or increased shortly before the event. These external conditions are understood to be conducive to substorm onsets (Lyons et al. 2005 and references therein).

3. Occurrence of extreme nighttime magnetic perturbation events

Table 2 shows the amplitude distributions of all nighttime intense magnetic perturbation events at each of the 8 stations during 2015 with peak to peak perturbation amplitude in any component $|\Delta B| > 200$ nT or peak derivative amplitude $|dB/dt| > 2$ nT/s. The number of events with perturbations in at least one component exceeding 200, 400, 600, and 1000 nT, as well as the value of the maximum perturbation, are shown in the left-hand columns, and the number of events with derivatives in at least once component exceeding 2, 4, 8, and 12 nT/s, as well as the value of the maximum derivative magnitude, are shown in the right-hand columns. Peak perturbations ranged from 957 nT to 2450 nT, nearly all in the X component, and peak derivative magnitudes ranged from 21.3 to 33.2 nT/s. Surprisingly, only at two stations were the largest derivative values in the X component; at five stations the largest value was in the Z (vertical) component. All of these maxima greatly exceed the commonly used threshold of 5 nT/s for potential damage to the electrical grid. For comparison, the Hydro Quebec collapse was associated with a storm-related dB/dt value of ~8 nT/s.

4. Association of nighttime magnetic perturbation events with Magnetic Storms

Figure 4 summarizes the temporal relations between magnetic storms and the largest nighttime events, showing that they were substantially different for occurrences of the largest peak to peak ΔB perturbations than for the largest amplitude derivatives (either positive or negative). In each of panels a-d of Figure 4 events are grouped in one of four categories: storm main phase, first day of recovery after a storm, non-storm times with -50 nT < Dst ≤ -15 nT (disturbed), and non-storm times with Dst > -15 nT (quiet). Only two |ΔB| > 1000 nT events and three |dB/dt| > 12 nT/s events occurred during the later recovery phase of a storm; these are not included in Figure 4 or in Figures S1 and S2 in the supplementary information. In this figure each event was counted only once, regardless of whether the amplitude threshold was exceeded in 1, 2, or 3 components.

Nearly 79% of the |ΔB| > 1000 nT events shown in Figure 4a occurred during storm main phase or the first day of the recovery phase, and only 21% during non-storm periods. A majority (56%) of the |dB/dt| > 12 nT/s events shown in Figure 4c also occurred during storms, but 44% occurred during non-storm periods.

It is important to note that nighttime events were still much more likely to occur during and immediately after magnetic storms than under quiet conditions, because these storms occurred during a relatively small fraction of the time. The amount of time during 2015 during which storm main phases occurred was 520 hours (~6 % of the year); thus the number of main phase events shown in panels a and c (18 each) greatly exceeds the number expected if these events occurred randomly during the year (2 in panel a and 5 in panel c). Similarly, the 40 days immediately after magnetic storms in 2015 are ~11% of the total days, so the number of events observed on these days (12 and 28) exceed the number expected for random occurrences (4 and 9, respectively) by a factor of ~3.

Panels b and d of Figure 4 show that nightside events at higher magnetic latitudes were also not as strongly associated with magnetic storms as those at lower latitudes. The occurrences of events with peak to peak ΔB amplitude > 1000 nT at the lower latitude stations (< 73° MLAT), shown in orange in panel b, occurred much more often during storm times (88%) than non-storm times (12%), and more often during the main phase than the first day of the recovery phase. At the higher latitude stations (73° MLAT), shown in blue in panel b, this ratio was only 62%, and as many events occurred during quiet conditions (4) as during storm main phase and first day of storm recovery (4 each). Panel d shows that more of the

|dB/dt| > 12 nT/s events at the lower latitude stations (orange) again occurred during storms (65%), but at the higher latitude stations (blue) only 42% occurred during storms, and 56% during non-storm intervals.

The Supporting Information contains two additional Figures, S1 and S2, that show event occurrences in a format similar to that of Figure 4, but displays events in the X, Y, and Z components separately as well as events in any component.

5. Comparison of 2015 and 2017 nighttime magnetic perturbation events at Repulse Bay

In an attempt to gain further insight into the relative importance of magnetic storms and substorms for nighttime event occurrence, event occurrences and amplitudes at MACCS station Repulse Bay (75.2° MLAT) were compared during 2015 and 2017, years with a greatly different number of magnetic storms. During 2015 there were a total of 40 storms (defined as having minimum Dst < -40 nT): 9 with minima between -40 and -49 nT, 21 with minima between -50 and -80 nT, 6 with minima between -80 and -120 nT, and 4 with minima < -120 nT. During 2017 there were a total of 15 such storms: 5 with minima between -40 and -49 nT, 8 with minima between -50 and -80 nT, 0 with minima between -80 and -120 nT, and 2 with minima < -120 nT.

Substorm onsets were identified for all nighttime events with peak to peak perturbation amplitude $\Delta B > 400$ nT or $|dB/dt| > 6$ nT/s in any component recorded at Repulse Bay, using the SuperMAG substorm data base. Figures 5a and 5b show the distribution of time delays between onset and all peak nighttime event derivatives ≥ 6 nT/s during 2015 and 2017, respectively. The pattern of time delays was nearly identical in both years: most of the events occurred between 0 and 30 minutes after onset (61% during 2015 and 62% during 2017), and an additional 24% in 2015 and 23% in 2017 occurred between 30 and 60 minutes after onset. Events occurring more than 1 hour after the closest prior substorm comprised 16% of the 2015 events and 15% of the 2017 events. One caveat should be mentioned: because the initiation of a new substorm may be masked by on-going activity during disturbed conditions, the time delays between substorm onsets and peak event derivatives may under these conditions be overestimates.

The distributions shown in Figures 5a and 5b can also be compared to what might be expected if the time delays between substorm onsets and nighttime magnetic perturbation event occurrences were random. The number of substorm onsets in the SuperMAG lists for years 2015 and 2017 are 1921 and 2093, indicating an average of 1 onset every 4.5 and 4.2 h, respectively. The number of nighttime event

occurrences within the first ½ hour after substorm onset if the events occurred randomly is 38 events * 0.5 h / 4.5 h ~4.2 events for 2015, and 47 events * 0.5 h / 4.2 h ~5.6 events for 2017. The resulting ratios between the actual and expected random numbers of events in the first ½ h for 2015 and 2017 are similar: 23/4.2 = 5.5 for 2015 and 29/5.6 = 5.2 for 2017.

Nighttime magnetic perturbation events at Repulse Bay were also separated into storm time and non-storm events. The distributions of these events were very similar for both years, so because of the modest number of events they have been combined in Figures 5c (storm time) and 5d (non-storm time). The number of storm time perturbation events (22) was only ~ 1/3 as large as the number of non-storm events (63). These panels show that most events in both categories occurred a few tens of minutes after substorm onset, but there was evidence of a long tail in both distributions as well.

Figure 6 shows a comparison of event perturbations (upper panels, a-f) and derivatives (lower panels, g-l) at Repulse Bay during 2015 and 2017 in three amplitude ranges as a function of storm phase (left panels, a-c and g-i) and time delay since substorm onset (right panels, d-f and j-l). Time delays from substorm onset between 0 to 30 min were classified as yes (Y), delays from 30 to 60 min as uncertain (?), and delays above 60 min as no (N). Storm events are grouped in 3 ranges: main phase and first day of recovery (left), second day of recovery (middle), and non-storm days.

Comparison of panels a and d of Figure 6 shows that although nearly equal numbers of nighttime events with peak to peak amplitudes > 800 nT occurred in association with storm times and non-storm times in both years, a substorm onset occurred from 5 to 30 min prior to every one of these events. Comparison of panels g and k again shows that all events with |dB/dt| > 12 nT/s occurred from 5 to 30 min after a substorm onset, and that the fraction of these events that occurred during storms dropped from 3/7 in 2015 to 1/7 in 2017.

The importance of storms relative to non-storm periods varied with event amplitude for both perturbations and derivatives: comparison of panels a-c shows a nearly constant number of storm-time events as their amplitude decreased, but more than a factor of 4 increase in non-storm time events. Comparison of panels g-i suggests a similar but weaker trend as a function of derivative amplitude.

Two other observations follow from a comparison of data for these two years. First, despite the dramatic drop in the number of magnetic storms from 2015 to 2017, the total number of events shown in Figures 5 and 6 increased from 37 to 46. The number of strongest events increased only slightly for both

perturbations and derivatives, but the lower amplitude events showed larger increases. Second, panels d-f and k-m show that the fraction of events that occurred after a longer time delay from substorm onset, and thus were less clearly associated with substorms, was larger during both years for the less intense events.

6. Spherical Elementary Current Systems Analysis

The spherical elementary current systems (SECS) technique developed by Amm and Viljanen (1999) uses vector magnetometer data from an array of ground stations to infer ionospheric equivalent vector currents, field-aligned currents, and horizontal components of the derivative of the magnetic field in the region covered by the measurements. Weygand et al (2011) implemented the SECS technique to produce maps of such currents over North America and Greenland, using data from 11 ground arrays: AUTUMNX, CARISMA, CANMOS, DTU, Falcon, GIMA, MACCS, McMAC, STEP, THEMIS, & USGS.

Figure 7 shows the results of a superposed epoch SECS analysis of 21 nighttime magnetic perturbation events observed at Cape Dorset between 0230 and 0330 UT, from mid-2014 through 2016. Figure 7a shows the magnetometers whose data were incorporated in this calculation, and median values from the set of events are shown in Figures 7b, c, and d. Figure 7b shows a strong electrojet current vortex centered east of Baffin Island, with the most intense current extending westward from western Greenland, over southern Baffin Island (including Cape Dorset) and northern Quebec, to the region north of Hudson Bay. Although in several of the 21 events the overhead equivalent current direction was consistent with the westward mean shown in Figure 7b, in many other cases the equivalent currents diverged poleward or equatorward just to the west of Cape Dorset (not shown).

The most intense westward currents in Figure 7b near Cape Dorset coincided with a region of shear between the strong downward and upward currents shown in Figure 7c, with Cape Dorset between them. Figure 7d shows a colored contour map of the intensity of the horizontal derivatives (in nT/s) at locations covered by these magnetometer arrays; the largest |dB/dt| values were located in this same region, but centered slightly south of Cape Dorset. This latitudinal deviation may be due to the fact that the 21 events were identified on the basis of large perturbation amplitudes at Cape Dorset rather than large dB/dt values. The median value of dB/dt did not exceed 2 nT/s, but several individual events did

exceed 2 nT/s. The intensity of the median dB/dt values dropped in half east and west from its maximum value over a distance of ~275 km.

7. Statistical Distributions of nighttime magnetic perturbation amplitudes

The form of the probability distribution function (PDF) $F(A)$ of a set of perturbation amplitudes A is determined by the physical mechanism of the process under study. A PDF and its moments are commonly used in the context of studies of turbulence. A non-gaussian distribution with a heavy tail indicates that the most intense fluctuations are not random, but are the result of the intermittency of the turbulence. The intermittency corresponds to turbulent processes where the rate of energy transfer is not constant, so periods of quiescence may change to bursts of activity (in particular, impulsive disturbances). The PDF of amplitude detection in the interval A, $A+dA$ is determined as the normalized number of events with amplitude $N(A)$:

$$n(A) = PDF(A) = \frac{N(A)}{N_t \Delta A}$$

Here N_t is the total number of events. The normalized histogram $n(A)$ provides the distribution of the probability to observe a given magnitude A in an interval ΔA during an analyzed period.

The cumulative amplitude distribution P(>A) (also known as the exceedance probability function or survival function) is determined as follows:

$$P(> A) = \int_A^\infty n(A) dA$$

The exceedance probability function $P(>A)$ is the probability to observe a value exceeding A. After evaluating and analyzing the statistical characteristics of the time series, one can speak about the similarity of their statistics, and consequently, about the similarity of their physical mechanisms.

We have compared the statistical distributions of magnetic perturbation amplitudes at different latitudes (stations IGL, SALU, and FCHU) from both 2015 and 2017. Only the values above the threshold ΔX=90 nT and dX/dt=0.8 nT/s have been accounted for. The PDFs at all stations were found to be close to the exponential-like distribution, though sometimes heavy tails (with few events) can be seen (Figures 8,9). We have attempted to find the same form of the approximation function for all stations. The difference between the parameters of these approximations provides a quantitative measure of the

difference between statistical properties of events at different latitudes. The analytical distribution function that fits best the measured PDF of both |ΔX| and |dX/dt| at all stations is the log-normal distribution

$$F(x,\sigma) = \frac{1}{x\sigma\sqrt{2\pi}} \exp\left(-\frac{\log^2(x)}{2\sigma^2}\right), \quad (2)$$

where σ is a shape parameter. While the PDF at a particular station could be slightly better approximated by another analytical function (e.g., the exponential Weibull distribution), in general (and especially for the heavy tails) the distributions are well approximated by (2).

To characterize quantitatively the deviation of the event statistics from the normal distribution of fluctuations, one may use the kurtosis *K*, which is determined via the statistical moments of the 2-nd order σ (standard deviation) and 4-th order μ_4 as follows: $K = \mu_4/\sigma^4 - 3$. For a normal Gaussian distribution $K = 0$. A distribution that is steeper and narrower than the normal one has $K > 0$, whereas a distribution with $K < 0$ is flatter than the normal one. We also have estimated the skewness value *S* that characterizes the asymmetry of the probability distributions. The parameters of the PDF at all stations are summarized in Table 3. Using these parameters, the difference between stations corresponding to different magnetospheric domains can be measured in a quantitative way.

The PDF of |ΔX| for all latitudes (IGL, SALU, FCHU) has about the same kurtosis *K* ~6-7 and skewness *S* ~1.8-1.9 (Table 3). High values of *K*>>1 for ΔB and dB/dt indicates that these distributions with long tail are the result of infrequent outliers. The PDF of |dX/dt| has the same *K* and *S* at $\Phi > 70^o$ (IGL,SALU), but lower values at latitude $\Phi < 70^o$ (FCHU). Such a difference may indicate that the statistics of |dX/dt| caused by nighttime magnetic perturbations at auroral latitudes differ from the statistics at latitudes poleward of the auroral oval.

The plots in Figures 8 and 9 also show the cumulative amplitude distributions P(>A). These exceedance probability distributions are well approximated by log-normal functions.

We have validated our statistical results by plotting the PDF of the absolute values of ΔB and dB/dt as follows: the magnetic field disturbance is determined as $\Delta B = \sqrt{(\Delta X)^2 + (\Delta Y)^2 + (\Delta Z)^2}$, and the field variability is characterized by the magnitude of the time derivative $\frac{dB}{dt} = \sqrt{(\frac{dX}{dt})^2 + (\frac{dY}{dt})^2 + (\frac{dZ}{dt})^2}$.

The PDF plots for station IGL (Figure 10) are qualitatively similar to the plots in Figures 8 and 9, and they are also well described by a log-normal distribution.

The tails of the PDFs in Figure 10 may be reasonably well approximated by a power function $f(A)=A^{-a}$, where A is an impulse amplitude, and a is an exponent. The power-law approximation (with a = 4.26) applied to tails of PDF of nighttime MIEs is very close to the log-normal approximation in this domain. Thus, the power-law may be a reasonable approximation in a rather narrow range of variables, while in a wider range of variables the power-law approximation is insufficient, and the PDF is better modeled by the log-normal distribution.

Knowledge of the PDF makes it possible to estimate the probability of an extreme event, which during the observation period may not even be observed (assuming that statistics of extreme events obeys the same law). The probabilities to detect impulses with the threshold dB/dt >10 nT/s are 12% at IGL; 11% at SALU; and 6.5 % at FCHU. Knowing the average number of events during a year, one may conclude that $201 \cdot 0.12/2 = 12$ impulses with amplitude above this threshold occur per year at IGL, $768 \cdot 0.11/2 = 42$ impulses at SALU, and $820 \cdot 0.065/2 = 27$ impulses at FCHU. The probabilities of extreme magnetic perturbations with dB/dt >50 nT/s are 0.007% at IGL; 0.005% at SALU; and 0.0006% at FCHU. Therefore, the expected annual rate of such extreme dB/dt values is 0.7 events per year at IGL; 1.9 events per year at SALU; and 0.25 events per year at FCHU.

The presence of heavy tails of a distribution is important. With such power distributions, the variance of a studied quantity is determined mainly by rare intense deviations, rather than by frequent small deviations. Mostly, heavy tails are noticeable in the distributions of |dX/dt|. Although there are indications of heavy tails in the distributions shown in Figures 8 and 9, the number of extreme events is too small to make any statistically significant conclusions.

8. Discussion

Although one might hope that the occurrence of the largest nighttime magnetic perturbation events would be consistently related to magnetospheric disturbances parameterized by geomagnetic storm indices such as Dst and SYM/H or substorm indices such as AE or SME, a substantial fraction of the nighttime events at the stations analyzed in this study occurred during non-storm and even non-substorm conditions. Although the fraction of large-amplitude perturbations ($\Delta B| > 1000$ nT) observed during non-

storm conditions at stations at latitudes <73° MLAT was lower than at the higher latitude stations, a substantial fraction of the largest amplitude derivatives (|dB/dt| > 12 nT/s) was observed during non-storm conditions in both latitude ranges, and the non-storm fraction exceeded the fraction during storms in the higher latitude range.

The maximum values shown in Table 2 can be compared to the maximum values of hourly range and rate of change recorded over a multi-year span at CANMOS observatories shown in Figures 8 and 9 of Nikitina et al. (2016). The maximum perturbation amplitudes recorded during 2015 are smaller than the maximum ranges at Fort Churchill during 41 years (2106 nT vs ~3500 nT) and Iqaluit during 17 years (1936 nT vs. ~5000 nT), but the maximum derivatives are slightly larger or comparable: 27.7 nT/s vs. ~18 nT/s at Fort Churchill and 22.3 nT/s vs. ~24 nT/s at Iqaluit. As Nikitina et al. (2016) noted, their results were based on 1-min data, which do not fully describe the shape of geomagnetic disturbances, so derivative values could well be different if derived from data sampled at a faster rate.

Two decades earlier, Viljanen (1997) compiled the maxima of dB/dt observed over a 5 ½ year interval in each of three geographic coordinate directions at 11 stations in the IMAGE array, at magnetic latitudes ranging from 56.8° to 76.1°. These maxima, based on data obtained with a 10 s sampling interval, are comparable both to the maxima reported here and to those reported by Nikitina et al. (2016). Similar to the results of Nikitina et al. (2016), the maxima generally increased as a function of magnetic latitude from the subauroral zone toward the polar cap, and similar to the results reported here, large derivatives could occur in any magnetic component.

The distribution of storm time and non-storm time delays of nighttime magnetic perturbation events after substorm onset shown in Figures 5c and 5d can be compared to those shown in Figure 3 of Viljanen et al. (2006). In that study the number of storm-time events was also much lower than the number of non-storm events at all three of the stations shown: Longyearbyen (75.12° MLAT, Sodanklyä (63.92° MLAT) and Nurmijärvi (56.89° MLAT). The distributions of both storm-time and non-storm events at Repulse Bay, with most events having delays between 0 and 40 minutes (Figures 5c and 5d), do not resemble the corresponding distributions at Longyearbyen (at similar magnetic latitude), which had broader distributions that extended to at least 90 minutes. The storm-time distributions at Sodanklyä and Nurmijärvi exhibited modest enhancements below 40 minutes delay, while the non-storm distributions were sharply peaked at 5 minutes delay and fell off rapidly to lower values at 20 minutes delay. The

distributions in Figures 5c and 5d appear to be intermediate between the storm time and non-storm distributions at Sodanklyä and Nurmijärvi in that most events occurred within 40 minutes after substorm onset. The distributions for both storm and non-storm times shown in both studies have long tails, which Viljanen et al. (2006) noted is typical for complex multiscale systems.

Viljanen et al. (2006) also noted that large dB/dt events were nearly always related to westward ionospheric currents, but the directional distributions of the horizontal time derivative vector (dH/dt) were much more scattered than those of the simultaneous horizontal variation field vector (H). They pointed out that this is possible only if there are rapidly changing ionospheric current systems of a length scale of 100 km or less embedded in a smooth background east-west flow. The data presented here are consistent with the Viljanen et al. (2006) observations. Table 2 shows that although the delta B maxima at all but one station are in the X direction, the directions are considerably more mixed for the maximum |dB/dt|. Figures S1 and S2 in the Supporting Information document the scarcity of > 1000 nT component perturbations in the Y component in both higher and lower MLAT ranges, in contrast to the occurrence of roughly half as many >12 nT/s derivatives in the Y component as in the X component. These figures also show that perturbations in the Z component have intermediate occurrence values: large ΔZ perturbations are more common than those in the Y component, and large |dZ/dt| are only slightly less common than |dX/dt|. In addition, as noted in section 6 above, the equivalent currents diverged poleward or equatorward in many of the Cape Dorset events included in the SECS superposed epoch analysis, but their median value pointed toward the west.

Viljanen et al. (2006) also suggested that the scattering of the directions of the maximum derivatives was related to smaller scale structures such as vortices. This is consistent with the earlier results of Apatenkov et al. (2004), who found, using IMAGE magnetometer data from 1996 through 2000, that the majority of the strongest dB/dt events appeared to be produced by vortex-type current structures. This conjecture was also confirmed by Belakhovsky et al. (2018), who found a much higher directional variability of the horizontal vector component of d**B**/dt compared to the horizontal component of Δ**B** during the magnetic storm of March 17, 2013.

The spatial scale of the enhanced horizontal dB/dt values shown in Figure 7d, ~275 km, can be compared to the observations of Ngwira et al. (2015). In that study, based on analysis of 12 extreme

geomagnetic storms between 1982 and 2005, the spatial range of the falloff of the geoelectric field (roughly proportional to dB/dt) exhibited large variations but was of the same order. Similar maps of SECS-determined dB/dt values shown in Paper 2 also fall in this range. In contrast, Sato et al. (1999) found dayside high-latitude MIE events to have smaller amplitudes but significantly larger spatial scales than reported here (~800 km latitudinal extent at half amplitude),

Ngwira et al. (2018) found that many extreme nighttime dB/dt variations at high latitudes were associated with poleward expanding discrete aurora passing over the magnetometer sites. In both of the two storm-time events studied, intense dB/dt events appeared near the poleward edge of the auroral zone and moved poleward as the auroral oval expanded poleward. They noted that this location is consistent with the observations of Wygant et al. (2000) that intense electric fields and Poynting flux occur at the poleward edge of the aurora. They also cautioned that it is not clear that substorms are themselves the primary seeding mechanism for strong dB/dt events, because substorms are widespread in nature but extreme dB/dt events are localized.

After evaluating and analyzing the statistical characteristics of the time series, one can speculate about their physical mechanisms. The fact that amplitudes of nightside magnetic perturbation events in the range of two orders of magnitude are described by the same law indicates that these impulsive disturbances are not accidental, but they are the manifestation of some organized physical process. The obtained probability distribution appears to be log-normal perhaps with some evidence of a high power tail which may indicate that this distribution is formed as a result of a multiplicative stochastic effect. Similarly, from 23-years statistics generated by using 10-s recordings from IMAGE magnetometers Pulkkinen et al. [2008] argued that the log-normal distribution characterizes the central properties of the dB/dt data well enough. On the other hand, analysis of 500 days of 10-s magnetic field recordings in the Quebec region showed that probability of having a disturbance of dB/dt exceeding a given threshold in the range from 0.05 nT/s to 10 nT/s was well approximated by a power law [Langlois et al., 1996]. However, because high field disturbances mostly occur in groups during strong magnetic storms, the statistics for extreme events may correspond to a single storm. Therefore, the statistics of pre-selected isolated nighttime magnetic perturbation events should not correspond to the statistics of magnetic field fluctuations.

Critical to enhancing understanding of magnetospheric dynamics is improved knowledge of how the energy stored in the magnetotail is transferred to energy released during substorms. The processes of the energy release in the magnetotail are turbulent, moreover turbulence has an intermittent character, that is, with a fluctuating rate of energy transfer from the driving scale of the spectra to the heating range of the spectrum (Consolini and De Michelis, 1998). Non-self-similar scaling of PDFs of the fluctuations in the flow or magnetic field was used to identify intermittent turbulence (Weygand et al., 2006). The magnetic fluctuations in the plasma sheet were found to be consistent with expectations for an intermittently turbulent MHD fluid (Weygand et al., 2005; Kozak et al., 2018). Stepanova et al. (2003) found that the PDF of the PC index (polar cap index charactering the energy supply from the solar wind into the magnetosphere) could be fitted by two log-normal distributions. On the basis of these results, it is possible to suggest that occurrence of nighttime magnetic perturbation events with log-normal statistics could be a reflection of intermittent turbulence of the magnetotail.

9. Summary

Observations of nighttime magnetic perturbation events from an extended array of ground-based magnetometers at magnetic latitudes above 68° showed that these events often have amplitudes that greatly exceed those associated with dayside transients (SIs, SSCs, and TCVs, stimulated by external perturbations originating in the solar wind or ion foreshock), and that these nighttime perturbations were temporally and well as spatially almost totally distinct from such dayside transients. This study provides additional evidence that many intense nighttime events occur at the poleward edge of the auroral zone, and that their correlation with magnetic storms is strongly dependent on a given station's magnetic latitude. This suggests that the statistical association of nighttime magnetic perturbation events with magnetic storms in some previous studies, often at lower latitudes, may be related to the expansion of the auroral oval to these latitudes.

The nighttime perturbation events in this study were often but not always associated with substorms, even when the substorms were identified using the SuperMAG database, which provides improved coverage at higher magnetic latitudes. Roughly 2/3 of the events observed at Repulse Bay (75° MLAT) during both 2015 and 2017 occurred less than 30 minutes after onset. No events were simultaneous with onsets, and a long-tailed distribution extending beyond several hours (also noted by

Viljanen et al., 2006) indicates that the association of nighttime magnetic perturbation events with substorms is not a simple one. Our observations also are in agreement with several recent studies that indicate that occurrences of the largest derivatives are not strongly coupled with occurrences of the largest magnetic deviations (and hence with the largest ionospheric currents). Taken together, these studies suggest that localized instabilities that commonly occur during substorms but can occur in association with other magnetotail phenomena may be the cause of the nighttime events. Two common features of all the nighttime events studied here, which must be considered when evaluating possible physical mechanisms for their generation, are their 5-10 min time scale and their ~300 km effective radius, which are evidently independent of their temporal relation to magnetic storms or substorms.

The statistical analyses presented in section 7 may also be of some help in efforts to determine the instabilities responsible for these highly localized nighttime perturbation events. Both analytical approximations and the higher-order parameters of the amplitude distributions indicate that the statistics of nighttime event amplitudes are similar at all 3 stations, ranging in MLAT from 67.7° to 77.6°, but exhibit a modest latitudinal trend in K and S for |dX/dt|. Comparison of the statistical distributions of impulse amplitudes of both |ΔX| and |dX/dt shows that PDFs at all stations fit well the log-normal distribution, and the kurtosis and skewness of the dX/dt| distributions confirms the conjecture that the statistics of nighttime event derivatives at auroral latitudes differs from those at higher latitudes. Also, the knowledge of the statistical characteristics of these events may enable a comparison to the statistics of relevant magnetospheric phenomena (substorm onsets, auroral streamers, BBFs, etc.) and hence the similarity of their physical mechanisms. According to many observations, intermittent turbulence of near-Earth plasma often has a log-normal form. A coincidence between the statistics of nightside perturbation events and magnetotail dynamics may indicate that the turbulence of the near-Earth plasma is largely responsible for the variability of the geomagnetic field on the time scale of these events (5-10 min).

Acknowledgements

We thank S. Ohtani for helpful comments. This work was supported by NSF grant AGS-1651263 to Augsburg University (MJE, VAP, LYA, JLP, ESS), NSF grant AGS-1654044 to the University of Michigan (MBM). NASA grants 80NSSC18K0570 and 80NSSC18K1220 and NASA contract NAS5-

02099 to UCLA (JMW), and a grant 16-17-00121 from the Russian Science Foundation (AVV). IRM was supported by the Natural Sciences and Engineering Research Council of Canada. We thank D.K. Milling and the rest of the CARISMA team for data. CARISMA is operated by the University of Alberta, funded by the Canadian Space Agency.

MACCS magnetometer data are available at http://space.augsburg.edu/maccs/requestdatafile.jsp, AUTUMNX data are available at http://autumn.athabascau.ca/, CANMOS data, provided by the Geological Survey of Canada, are available at http://geomag.nrcan.gc.ca/data-donnee/sd-en.php, and CARISMA data are available at http://www.carisma.ca/carisma-data-repository. The SME index is available from SuperMAG (http://supermag.jhuapl.edu/indices/), PI J. Gjerloev), derived from magnetometer data from Intermagnet; USGS, J.J. Love; CARISMA, PI I. Mann; CANMOS, Geomagnetism Unit of the Geological Survey of Canada; The S-RAMP Database, PI K. Yumoto and K. Shiokawa; The SPIDR database; AARI, PI O. Troshichev; The MACCS program, PI M. Engebretson; GIMA; MEASURE, UCLA IGPP and Florida Institute of Technology; 210 Chain, PI K. Yumoto; SAMNET, PI F. Honary; The institutes who maintain the IMAGE magnetometer array, PI E. Tanskanen; PENGUIN; AUTUMN, PI M. Connors; DTU Space, PI Dr. R. Behlke; South Pole and McMurdo Magnetometer, PI's L.J. Lanzerotti and A.T. Weatherwax; ICESTAR; RAPIDMAG; PENGUIn; British Artarctic Survey; McMAC, PI P. Chi; BGS, PI Dr. S. Macmillan; Pushkov Institute of Terrestrial Magnetism, Ionosphere and Radio Wave Propagation (IZMIRAN); GFZ, PI Dr. Juergen Matzka; MFGI, PI B. Heilig; IGFPAS, PI J. Reda; University of L'Aquila, PI M. Vellante.

References

Amm, O., and A. Viljanen (1999), Ionospheric disturbance magnetic field continuation from the ground to the ionosphere using spherical elementary currents systems, *Earth Planets Space, 51,* 431–440.

Apatenkov, S. V., V. A. Sergeev, R. Pirjola, and A. Viljanen (2004), Evaluation of the geometry of ionospheric current systems related to rapid geomagnetic variations, *Ann. Geophys., 22,* 63-72, https://doi.org/10.5194/angeo-22-63-2004.

Belakhovsky, V. B., V. A. Pilipenko, Y. A. Sakharov, and V. N. Selivanov (2018), Characteristics of the variability of a geomagnetic field for studying the impact of the magnetic storms and substorms on electrical energy systems, *Izvestiya, Physics of the Solid Earth, 54*, 52–65, ISSN 1069-3513.

Boteler, D. H., R. J. Pirjola, and H. Nevanlinna (1998), The effects of geomagnetic disturbances on electrical systems at the Earth's surface, *Adv. Space Res*. 22, 17-27

Connors, M., I. Schofield, K. Reiter, P. J. Chi, K. M. Rowe, and C. T. Russell (2016), The AUTUMNX magnetometer meridian chain in Québec, Canada, *Earth, Planets and Space, 68:2*, DOI 10.1186/s40623-015-0354-4.

Consolini, G., and P. De Michelis (1998), Non-Gaussian distribution function of AE index fluctuations: Evidence for time intermittency, *Geophys. Res. Lett., 25*, 4087–4090, doi:10.1029/1998GL900073.

Engebretson, M. J., W. J. Hughes, J. L. Alford, E. Zesta, L. J. Cahill Jr., R. L. Arnoldy, and G. D. Reeves (1995), Magnetometer array for cusp and cleft studies observations of the spatial extent of broadband ULF magnetic pulsations of cusp/cleft latitudes, *J. Geophys. Res., 100,* 19371-19386, doi:10.1029/95JA00768.

Engebretson, M. J., T. K. Yeoman, K. Oksavik, F. Søraas, F. Sigernes, J. I. Moen, M. G. Johnsen, V. A. Pilipenko, J. L. Posch, M. R. Lessard, B. Lavraud, M. D. Hartinger, L. B. N. Clausen, T. Raita, and C. Stolle, (2013), Multi-instrument observations from Svalbard of a traveling convection vortex, electromagnetic ion cyclotron wave burst, and proton precipitation associated with a bow shock instability, *J. Geophys. Res. Space Physics, 118*, 2975-2997, doi:10.1002/jgra.50291.

Engebretson, M. J., E. S. Steinmetz, J. L. Posch, V. A. Pilipenko, M. B. Moldwin, M. G. Connors, D. H. Boteler, I. R. Mann, M. D. Hartinger, J. M. Weygand, L. R. Lyons, Y. Nishimura, H. J. Singer, S. Ohtani, C. T. Russell, A. Fazakerley, and L. M. Kistler, Nighttime magnetic perturbation events

observed in Arctic Canada, 2, Multiple-instrument observations, revised version to be submitted to the *Journal of Geophysical Research – Space Physics,* 2019.

Friis-Christensen E., M.A. McHenry, C.R. Clauer, S. Vennerstrøm (1988), Ionospheric traveling convection vortices observed near the polar cleft: A triggered response to sudden changes in the solar wind, *Geophys. Res. Lett. 15,* 253-256, doi:10.1029/GL015i003p00253.

Kappenman, J.G. (2005), An overview of the impulsive geomagnetic field disturbances and power grid impacts associated with the violent sun-earth connection events of 29-31 October 2003 and a comparative evaluation with other contemporary storms, *Space Weather*, *3* (8), S08C01, doi:10.1029/2004SW000128.

Kataoka, R., H. Fukunishi, and L. J. Lanzerotti (2003), Statistical identification of solar wind origins of magnetic impulse events, *J. Geophys. Res.*, *108,* 1436, doi:10.1029/2003JA010202.

Knipp, D.J. (2015), Synthesis of geomagnetically induced currents: Commentary and research, *Space Weather*, *13* (11), 727-729, doi:10.1002/2015SW001317.

Kozak L.V., B.A. Petrenko, A. T. Y. Lui, E.A. Kronberg, E.E. Grigorenko, and A.S. Prokhorenkov, Turbulent processes in the Earth's magnetotail: spectral and statistical research, *Ann. Geophys.*, *36*, 1303–1318, 2018, https://doi.org/10.5194/angeo-36-1303-2018.

Kozyreva, O. V., V. A. Pilipenko, V. B. Belakhovsky, and Ya. A. Sakharov (2018), Ground geomagnetic field and GIC response to March 17, 2015, storm, *Earth, Planets and Space, 70:157,* doi: 10.1186/s40623-018-0933-2.

Langlois P., L. Bolduci, and M.C. Chouteau (1996), Probability of occurrence of geomagnetic storms based on a study of the distribution of the electric field amplitudes measured in Abitibi, Quebec, in 1993-94, *J. Geomag. Geoelectr.*, *48*, 1033-1041.

Lanzerotti, L. J., A. Wolfe, N. Trivedi, C. G. Maclennan, and L. V. Medford (1990), Magnetic impulse events at high latitudes: magnetopause and boundary layer plasma processes, *J. Geophys. Res.*, *95*, 97-107, https://doi.org/10.1029/JA095iA01p00097.

Lanzerotti L.J. (2001), Space weather effects on technologies, *Space Weather, Geophys. Monogr. Ser*. AGU. vol. 125, p. 11.

Lyons, L. R., D.-Y. Lee, C.-P. Wang, and S. B. Mende (2005), Global auroral responses to abrupt solar

wind changes: Dynamic pressure, substorm, and null events, *J. Geophys. Res., 110*, A08208, doi:10.1029/2005JA011089.

Mann, I. R., et al. (2008), The upgraded CARISMA magnetometer array in the THEMIS era, *Space Sci. Rev., 141*, 413–451, doi:10.1007/s11214-008-9457-6.

Ngwira, C. M., A. A. Pulkkinen, E. Bernabeu, J. Eichner, A. Viljanen, and G. Crowley (2015), Characteristics of extreme geoelectric fields and their possible causes: Localized peak enhancements, *Geophys. Res. Lett., 42*, 6916–6921, doi:10.1002/2015GL065061.

Ngwira C. M., D. G. Sibeck, M. D. V. Silveira, M. Georgiou, J. M. Weygand, Y. Nishimura, and D. Hampton (2018). A study of intense local *dB/*d*t* variations during two geomagnetic storms. *Space Weather*, *16*, 676–693, doi:10.1029/2018SW001911.

Nikitina, L., L. Trichtchenko, and D. H. Boteler (2016), Assessment of extreme values in geomagnetic and geoelectric field variations for Canada, *Space Weather, 14*, 481–494, doi:10.1002/2016SW001386.

Pulkkinen, A., M. Hesse, M. Kuznetsova, and L. Rastätter (2007), First-principles modeling of geomagnetically induced electromagnetic fields and currents from upstream solar wind to the surface of the Earth, *Ann. Geophys., 25*, 881–893, doi:10.5194/angeo-25-881-2007.

Pulkkinen, A., R. Pirjola, and A. Viljanen (2008), Statistics of extreme geomagnetically induced current events, *Space Weather, 6*, S07001, doi:10.1029/2008SW000388.

Sato, M., Fukunishi, H., Lanzerotti, L. J., and Maclennan, C. G. (1999), Magnetic impulse events and related Pc1 bursts observed by the Automatic Geophysical Observatories network in Antarctica, J. Geophys. Res., 104, 19971- 19982, doi:10.1029/1999JA900111.

Stepanova, M. V., E. E. Antonova, and O. Troshichev (2003), Intermittency of magnetospheric dynamics through non-Gaussian distribution function of PC-index fluctuations, *Geophys. Res. Lett., 30*, 1127, doi:10.1029/2002GL016070.

Viljanen A. (1997), The relation between geomagnetic variations and their time derivatives and implications for estimation of induction risks, *Geophys. Res. Lett., 24*, 631-634, doi:10.1029/97GL00538.

Viljanen, A., (1998), Relation of geomagnetically induced currents and local geomagnetic field variations, *IEEE Transactions on Power Delivery*, *13*, 1285-1290.

Viljanen, A., E. I. Tanskanen, and A. Pulkkinen (2006), Relation between substorm characteristics and

rapid temporal variations of the ground magnetic field, *Ann. Geophys., 24*, 725-733, doi:10.5194/angeo-24-725-2006.

Vorobjev, V. G., V. L. Zverev, and G. V. Starkov (1993), Geomagnetic impulses in day-side high latitude region: main morphological characteristics and relation with dynamics of dayside aurora, *Geomagn. Aeronomy, 33,* 69-79.

Weygand, J. M., M. G. Kivelson, K. K. Khurana, H. K. Schwarzl, S.M. Thomson, R.L. McPherron, A. Balogh, L. M. Kistler, and M. L. Goldstein (2005), Plasma sheet turbulence observed by Cluster II, *J. Geophys. Res., 110,* A01205, doi:10.1029/2004JA010581.

Weygand, J. M., M. G. Kivelson, K. K. Khurana, H. K. Schwarzl, R. J. Walker, A. Balogh, L. M. Kistler, and M. L. Goldstein (2006), Non-self-similar scaling of plasma sheet and solar wind probability distribution functions of magnetic field fluctuations, *J. Geophys. Res., 111,* A11209, doi:10.1029/2006JA011820.

Weygand, J. M., O. Amm, A. Viljanen, V. Angelopoulos, D. Murr, M. J. Engebretson, H. Gleisner, and I. R. Mann (2011), Application and validation of the spherical elementary currents systems technique for deriving ionospheric equivalent currents with the North American and Greenland ground magnetometer arrays, *J. Geophys. Res., 116,* A03305, doi:10.1029/2010JA016177.

Wygant, J. R., A. Keiling, C. A. Cattell, M. Johnson, R. L. Lysak, M. Temerin, F. S. Mozer, C. A. Kletzing, J. D. Scudder, W. Peterson, C. T. Russell, G. Parks, M. Brittnacher, G. Germany, and J. Spann (2000), Polar spacecraft based comparisons of intense electric fields and Poynting flux near and within the plasma sheet-tail lobe boundary to UVI images: An energy source for the aurora, *J. Geophys. Res., 105,* 18,675–18,692, doi:10.1029/1999JA900500.

Zhang, J. J., C. Wang, and B. B. Tang (2012), Modeling geomagnetically induced electric field and currents by combining a global MHD model with a local one-dimensional method, *Space Weather,10,* S05005, doi:10.1029/2012SW000772.

Table 1. Stations used in this study.

Array	Station	Code	Geog. Lat.	Geog. Lon.	CGM Lat,	CGM Lon.	Cadence
MACCS	Igloolik	IGL	69.3°	278.2°	77.6°	-5.0°	0.5s
	Repulse Bay	RBY	66.5°	273.8°	75.2°	-12.8°	0.5s
	Pangnirtung	PGG	66.1°	294.2°	73.3°	19.8°	0.5s
	Cape Dorset	CDR	64.2°	283.4°	72.7°	3.0°	0.5s
AUTUMNX	Salluit	SALU	62.2°	284.3°	70.7°	4.1°	0.5s
CANMOS	Iqaluit	IQA	63.8°	291.5°	71.4°	15.1°	1.0s
	Fort Churchill	FCHU	58.8°	265.9°	67.7°	-24.6°	1.0s
CARISMA	Rankin Inlet	RANK	62.8°	267.9°	71.7°	-22.2°	1.0s

Corrected magnetic (CGM) coordinates are for epoch 2015, using http://sdnet.thayer.dartmouth.edu/aacgm/aacgm_calc.php#AACGM .

Table 2. Numbers of nighttime magnetic perturbation events at each station that exceeded the given ΔB or dB/dt value in any component during 2015.

STA	>200nT	>400nT	>600nT	>1000nT	Max ΔB	>2nT/s	>4nT/s	>8nT/s	>12nT/s	Max dB/dt
IGL	67	25	13	2	2304 X	58	28	8	4	21.3 Z
RBY	171	55	21	3	1439 X	140	69	19	7	23.6 Z
PGG	199	82	31	3	1026 X	209	122	37	14	30.9 X
CDR	223	86	36	8	2248 Z	220	118	34	8	33.2 X
RANK	286	137	58	10	2450 X	273	143	49	18	24.3 Z
IQA	337	141	39	7	1936 X	349	186	34	9	22.3 Y
SALU	202	79	23	1	957 X	204	112	29	12	25.6 Z
FCHU	322	144	61	11	2106 X	299	137	44	11	27.7 Z

Table 3. Parameters of the probability distribution function (PDF) for a log-normal distribution.

parameter / Station/Φ	$\lvert\Delta X\rvert$			$\lvert dX/dt\rvert$		
	σ	*K*	*S*	σ	*K*	*S*

IGL (77.6°)	0.53	7.0	1.9	0.66	14.3	2.6
SALU (70.7°)	0.50	6.0	1.8	0.65	13.9	2.6
FCHU (67.7°)	0.53	6.9	1.9	0.60	10.5	2.3

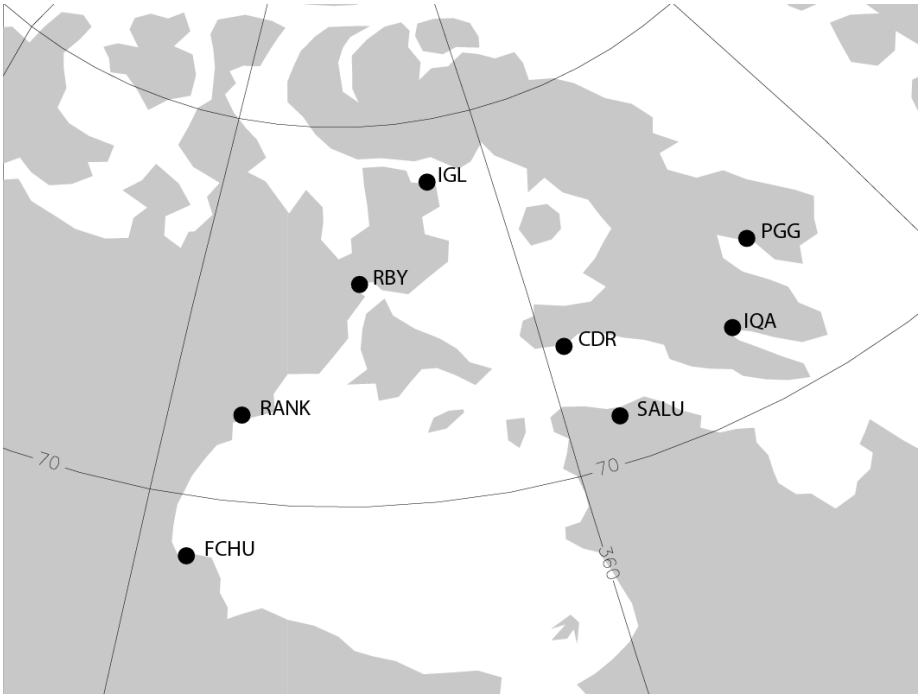

Figure 1. Map of Eastern Arctic Canada showing the locations of the 8 ground magnetometers used in this study.

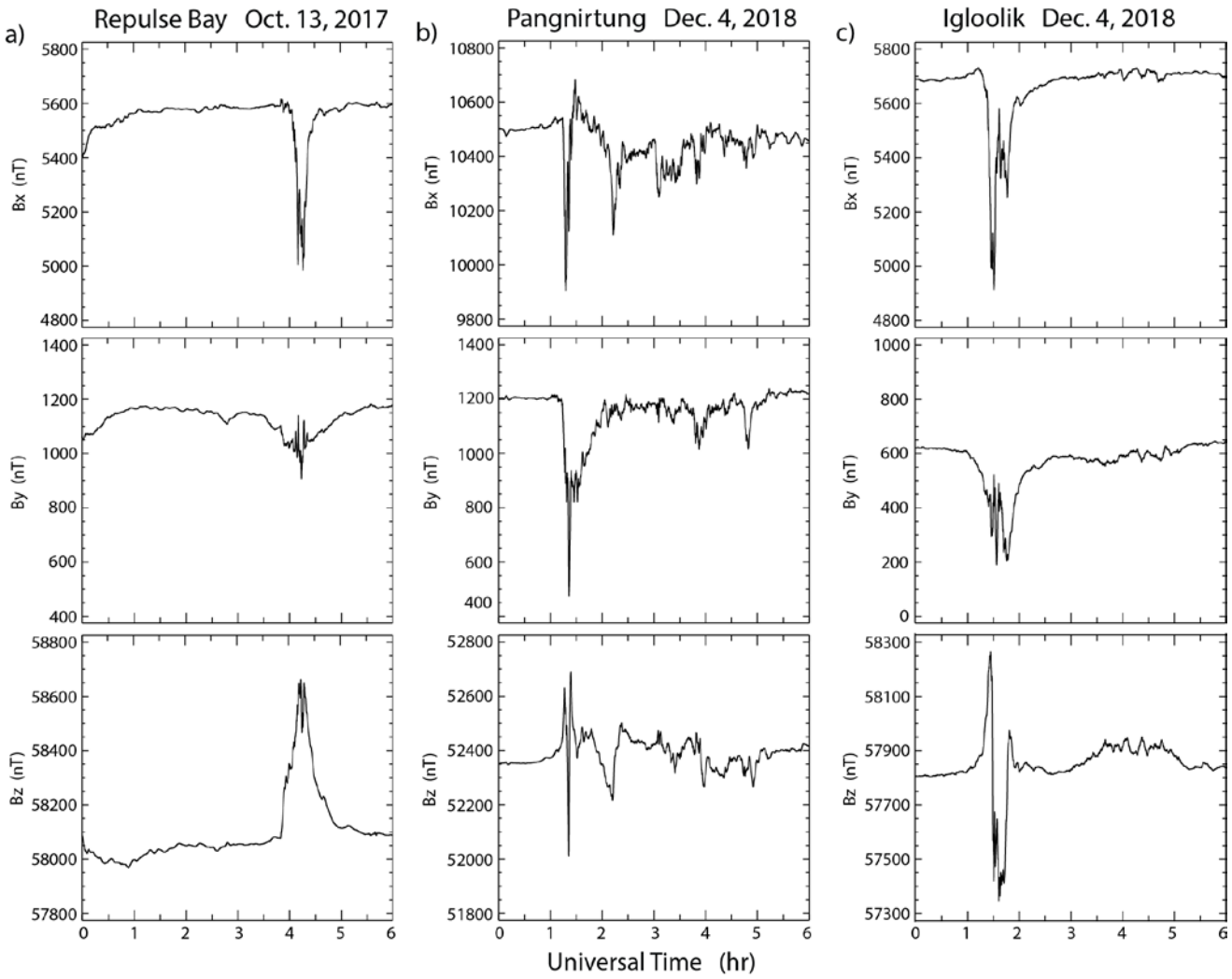

Figure 2: Six-hour excerpts from three daily magnetograms, each showing large nighttime magnetic perturbations: Repulse Bay Oct. 13, 2017; and Pangnirtung and Igloolik Dec. 4, 2018, each showing large solitary magnetic impulses in both the X (north-south) and Z (vertical) components. Derivatives at Pangnirtung exceeded 10 nT/s in all 3 components, and were largest in Z (+13 nT/s).

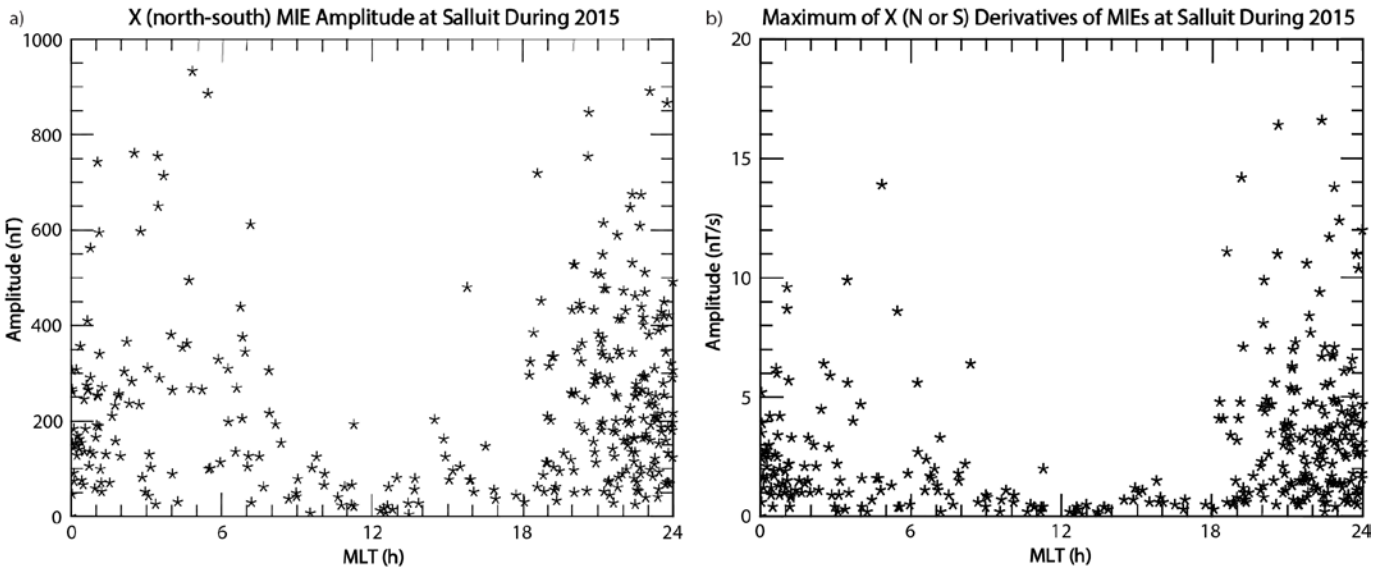

Figure 3. Scatter plots of the peak to peak amplitudes (panel a) and maximum (positive or negative) derivatives (panel b) of the X (north-south) component of magnetic perturbations events identified at Salluit during 2015 as a function of magnetic local time.

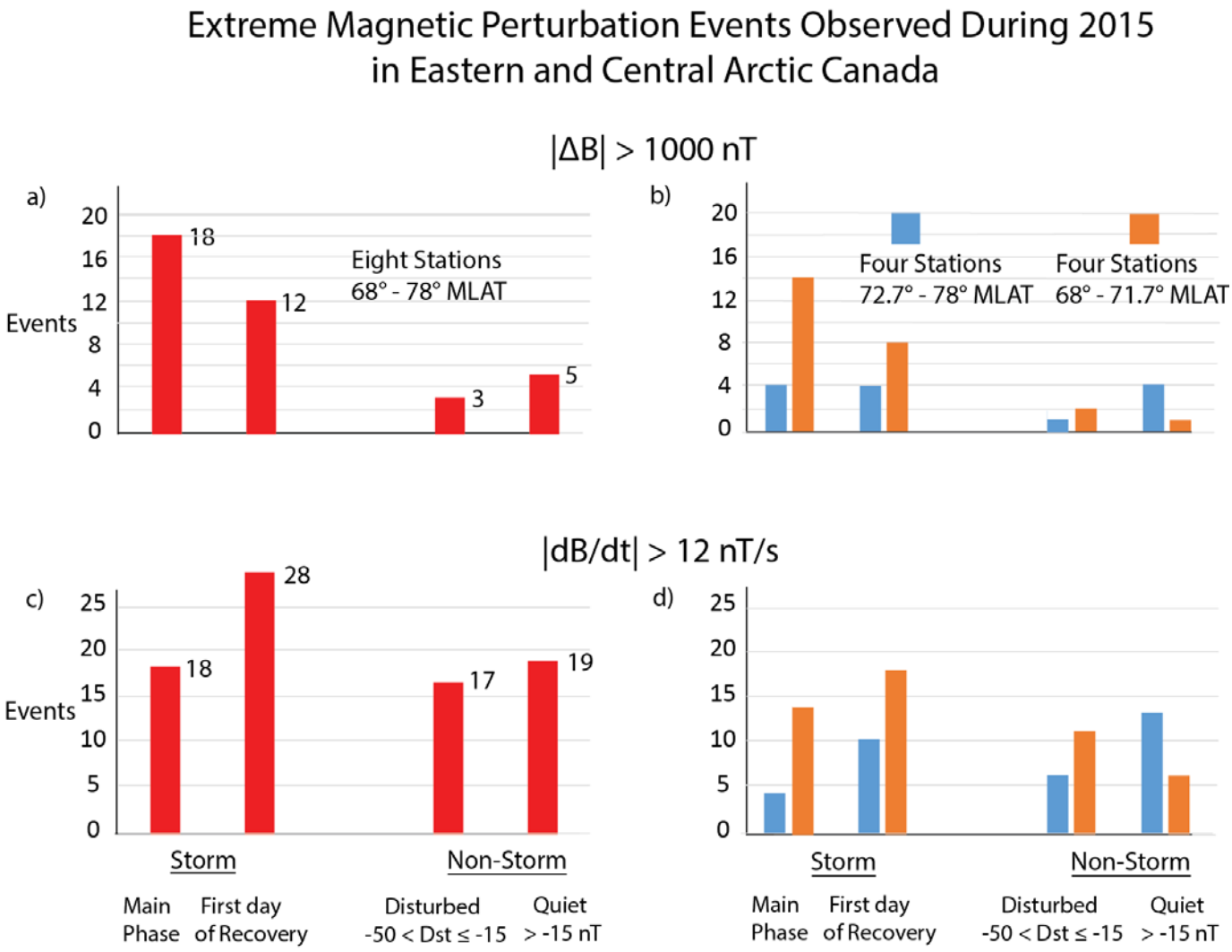

Figure 4. Bar plots of occurrences of extreme magnetic perturbation events observed during 2015 in Eastern and Central Arctic Canada. Panels a and c show the number of events with peak to peak excursions of the magnetic field exceeding 1000 nT in any component, and panels b and d show the number of events with peak time derivatives of the magnetic field (either positive or negative) exceeding 12 nT/s. Events are separated into four storm phase categories, as described in the text.

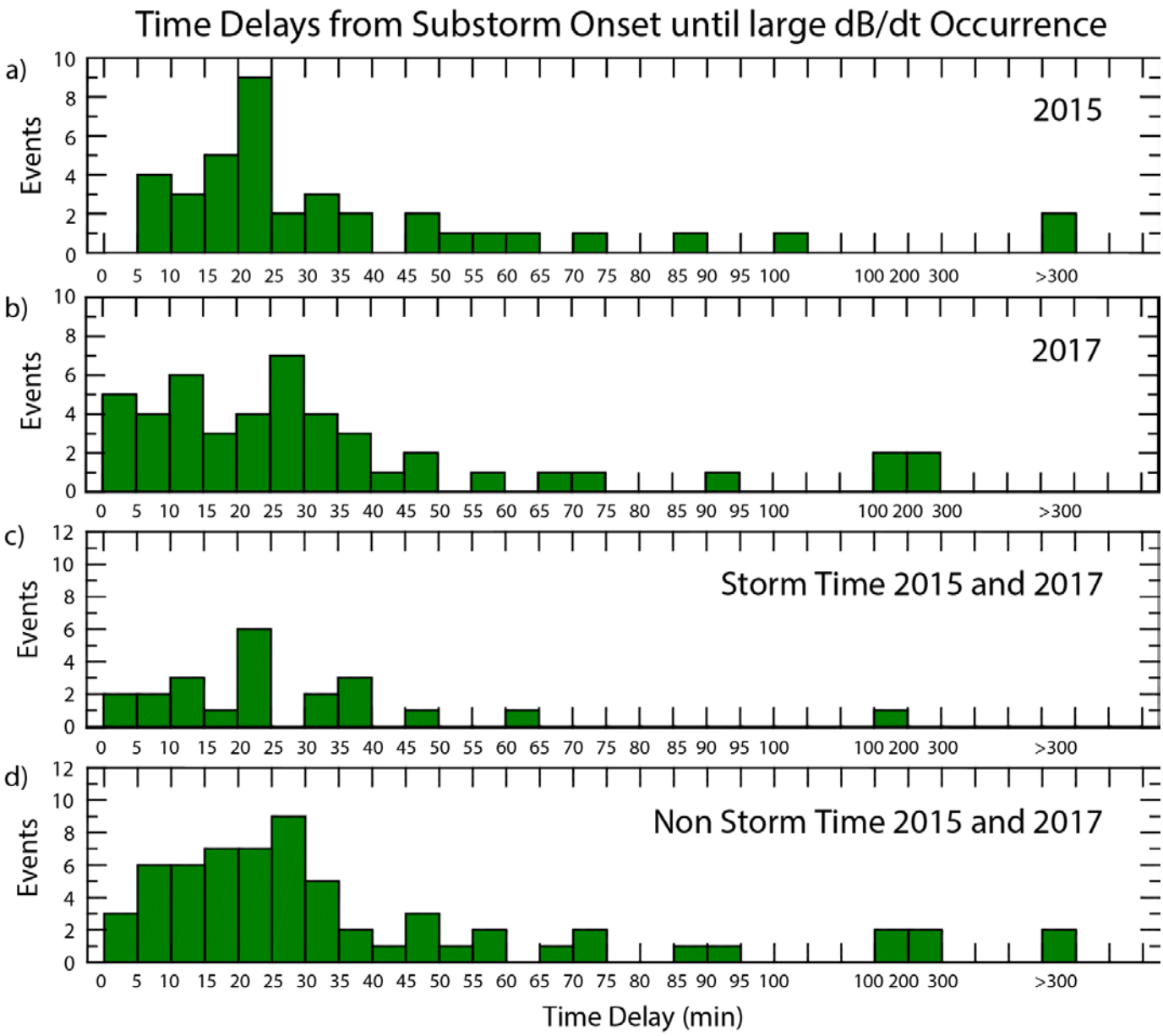

Figure 5. Histograms of time delays between substorm onsets and > 6 nT/s amplitude nighttime magnetic perturbation events observed at Repulse Bay. Panel a: all events during 2015. Panel b: all events during 2017. Panel c: events during magnetic storms during both 2015 and 2017. Panel d: events during non-storm times during both 2015 and 2017.

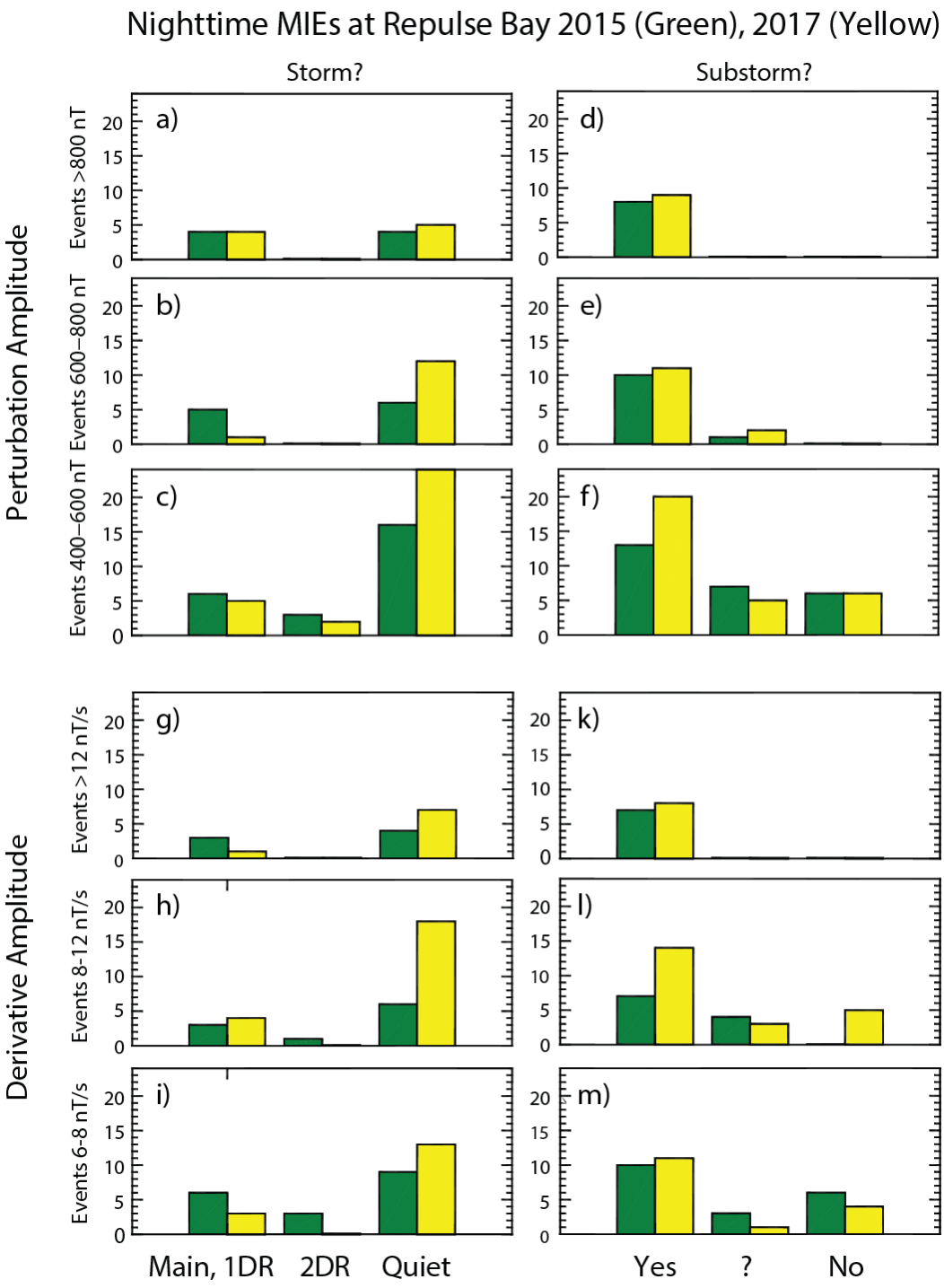

Figure 6. Comparisons of the occurrences of nighttime magnetic perturbation events (upper panels) and derivatives (lower panels) at Repulse Bay during 2015 and 2017 in three amplitude ranges as a function of storm phase (left panels) and time delay since substorm onset (right panels). Panels a-c and d-f show the

number of events in three perturbation amplitude ranges: 400-600 nT, 600-800 nT, and > 800 nT, and panels g-i and j-l show the number of events in three derivative amplitude ranges: -8 nT/s, 8-12 nT/s, and > 12 nT/s. Storm events are grouped in 3 categories: main phase and first day of recovery (left), second day of recovery (middle), and non-storm days (right). Time delays from substorm onset between 0 to 30 min were classified as Yes, delays from 30 to 60 min as uncertain (?), and delays above 60 min as No.

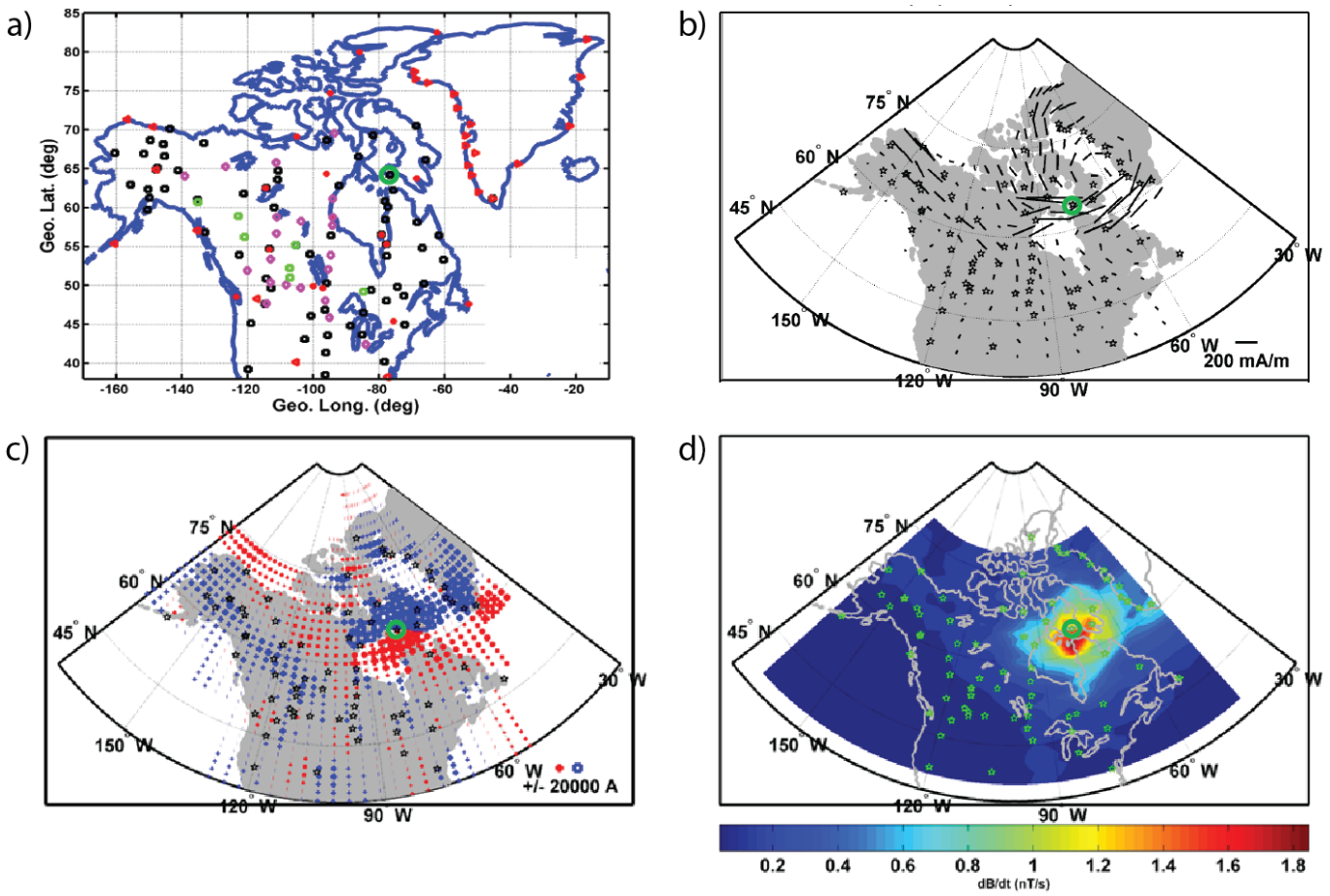

Figure 7. Panel a: Map showing the magnetometers used for the SECS superposed epoch analysis of 21 large nighttime magnetic perturbation events observed at Cape Dorset from mid-2014 through 2016. Panels b-d show median values of equivalent ionospheric currents, inferred field-aligned currents, and horizontal components of the derivative of the magnetic field (dB/dt) in nT/s, respectively. Stars in panels b-d indicate some (but not all) of the stations used in the analysis, and Cape Dorset is marked by an open green circle. The length of the vectors in panel b indicates the magnitude of the current according to the scale at the lower right. The red plus symbols in panel c indicate downward currents, which are the positive directions for the model, and blue squares indicate upward currents. The size of the symbol indicates the magnitude of the current according to the scale at the lower right. The amplitude of the horizontal derivative in panel d is coded according to the color bar below it.

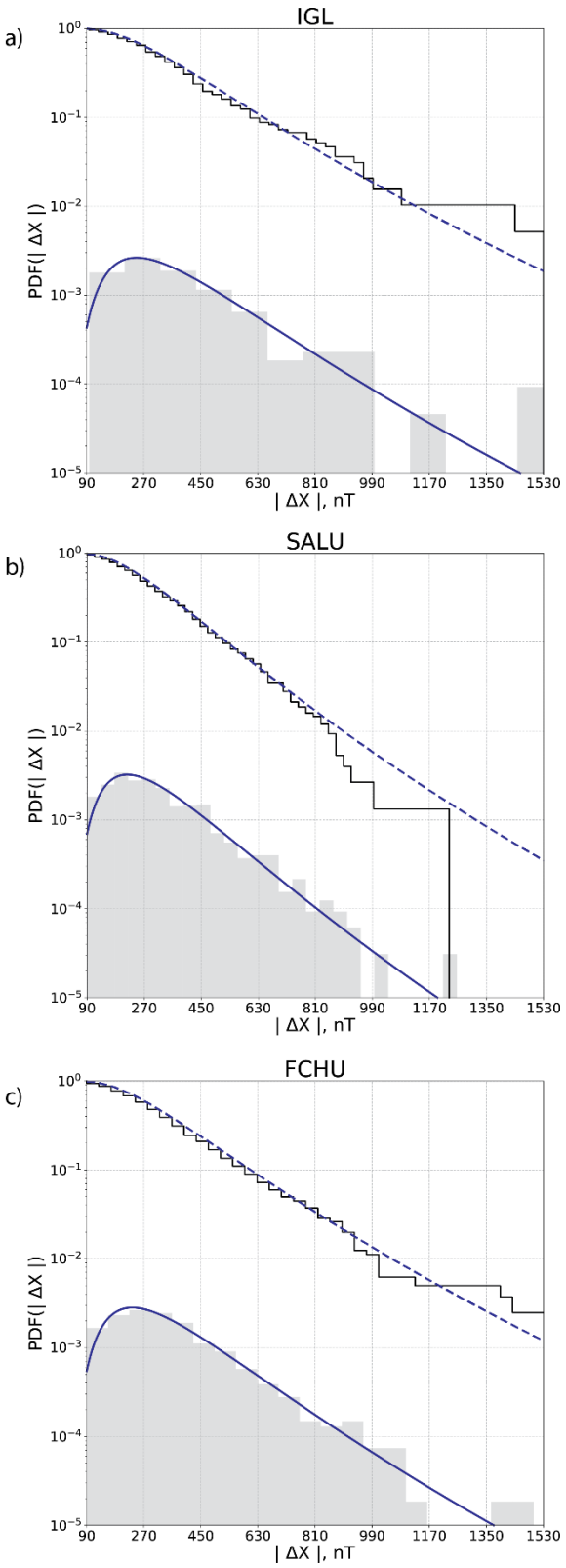

Figure 8. Plots for |ΔX| of histograms of the probability distribution PDF(A) (grey bars) and cumulative distribution (exceedance function) $P(>A) = \int_A^\infty n(A)dA$ (solid black lines) of data from Igloolik (panel a), Salluit (panel b), and Fort Churchill (panel c). The best fit log-normal approximations are solid blue lines for |ΔX|, and dashed blue lines for P(>ΔX).

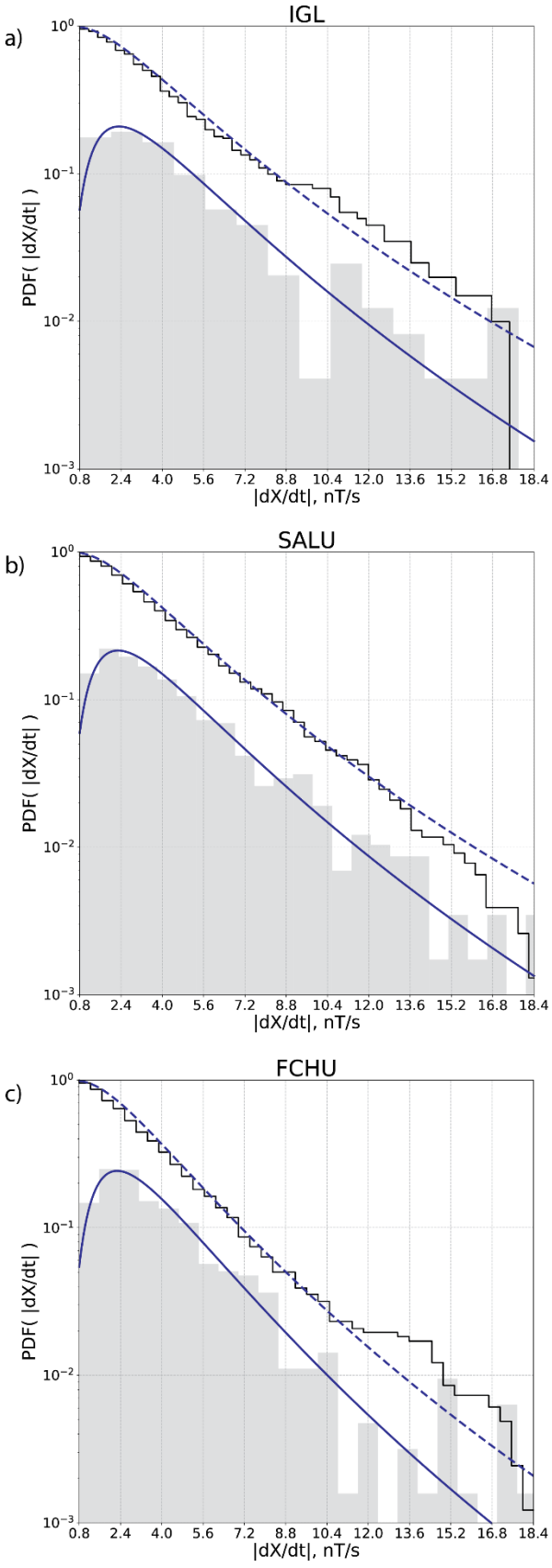

Figure 9. The same format as in Fig. 8, but for |dX/dt|.

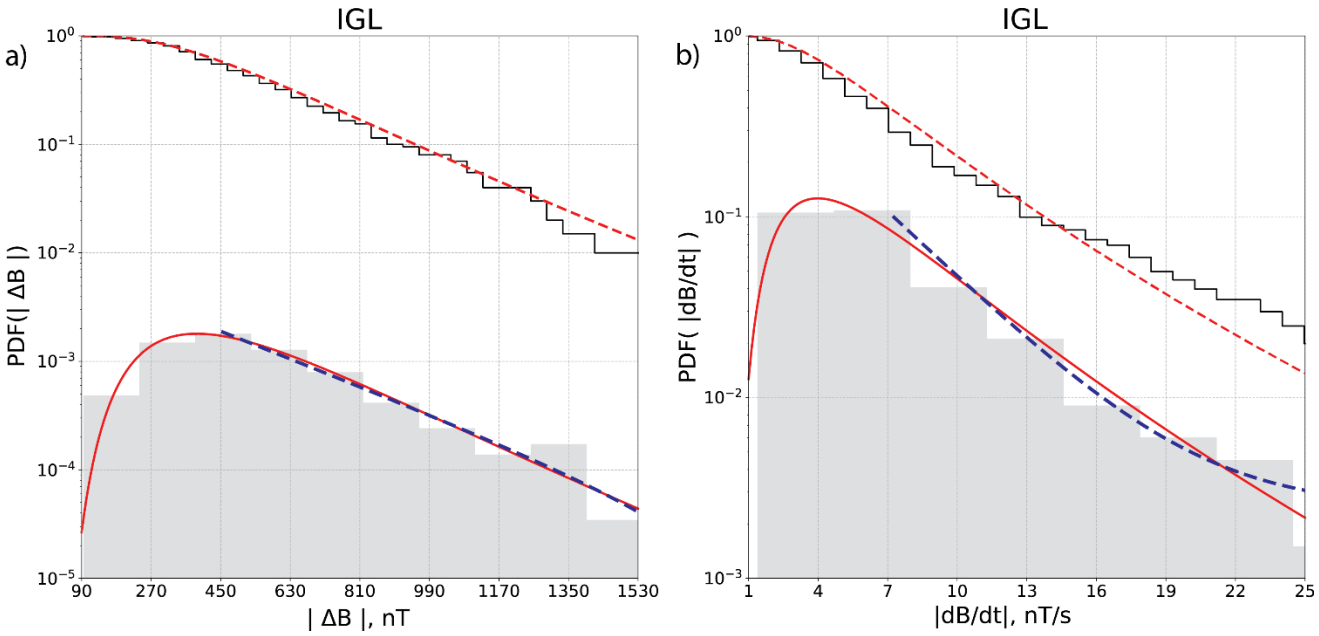

Figure 10. Panel a: Histograms of the probability distribution PDF (ΔB) (grey bars) and cumulative distribution (exceedance function) *P*(>ΔB) (solid black lines) of data from Igloolik. The best fit log-normal approximations are denoted by solid red lines for ΔB and dashed red lines for P(>ΔB). Panel b: The same format, but for dB/dt. In both panels the blue dashed lines show the power-law approximation of the distribution tails.

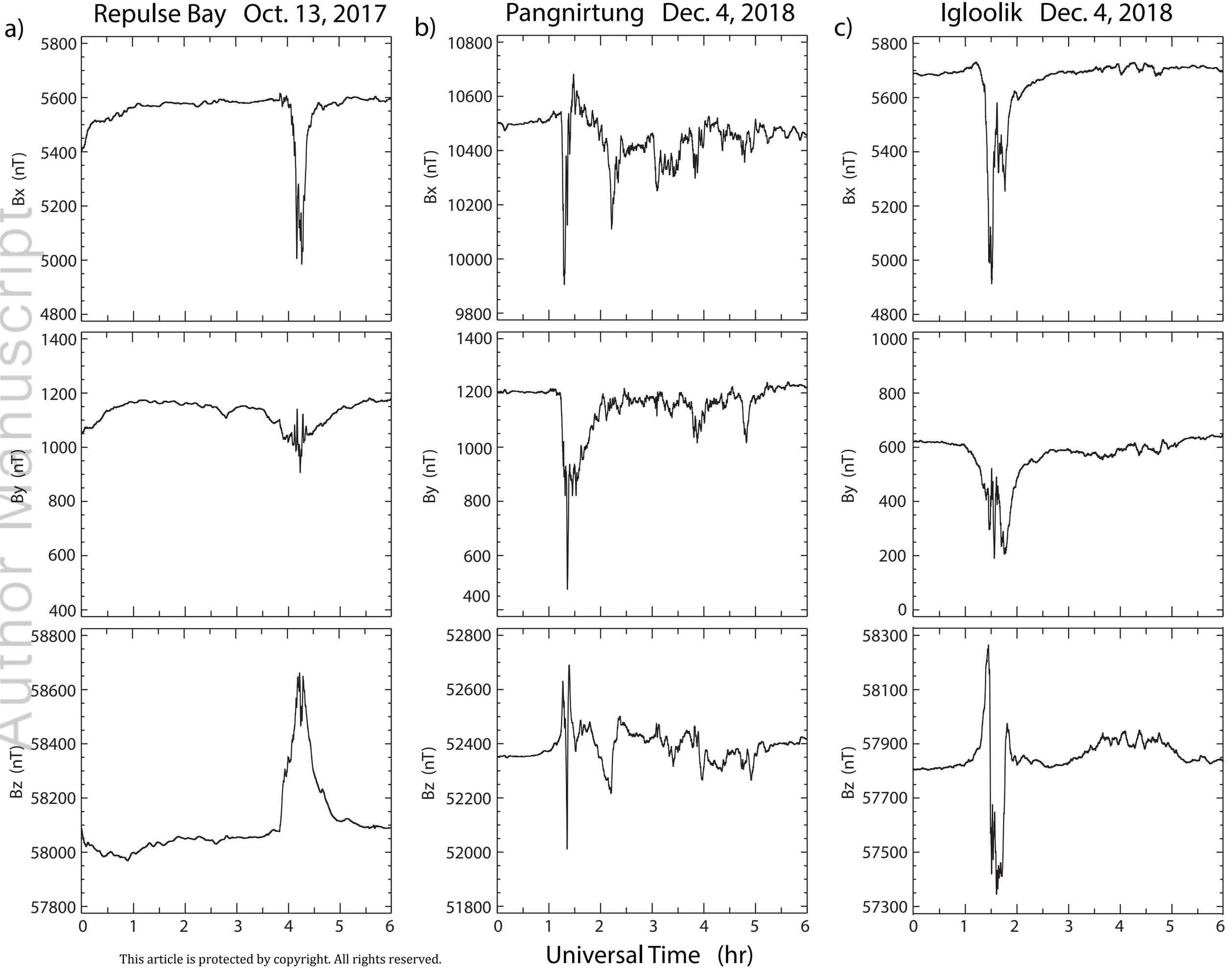

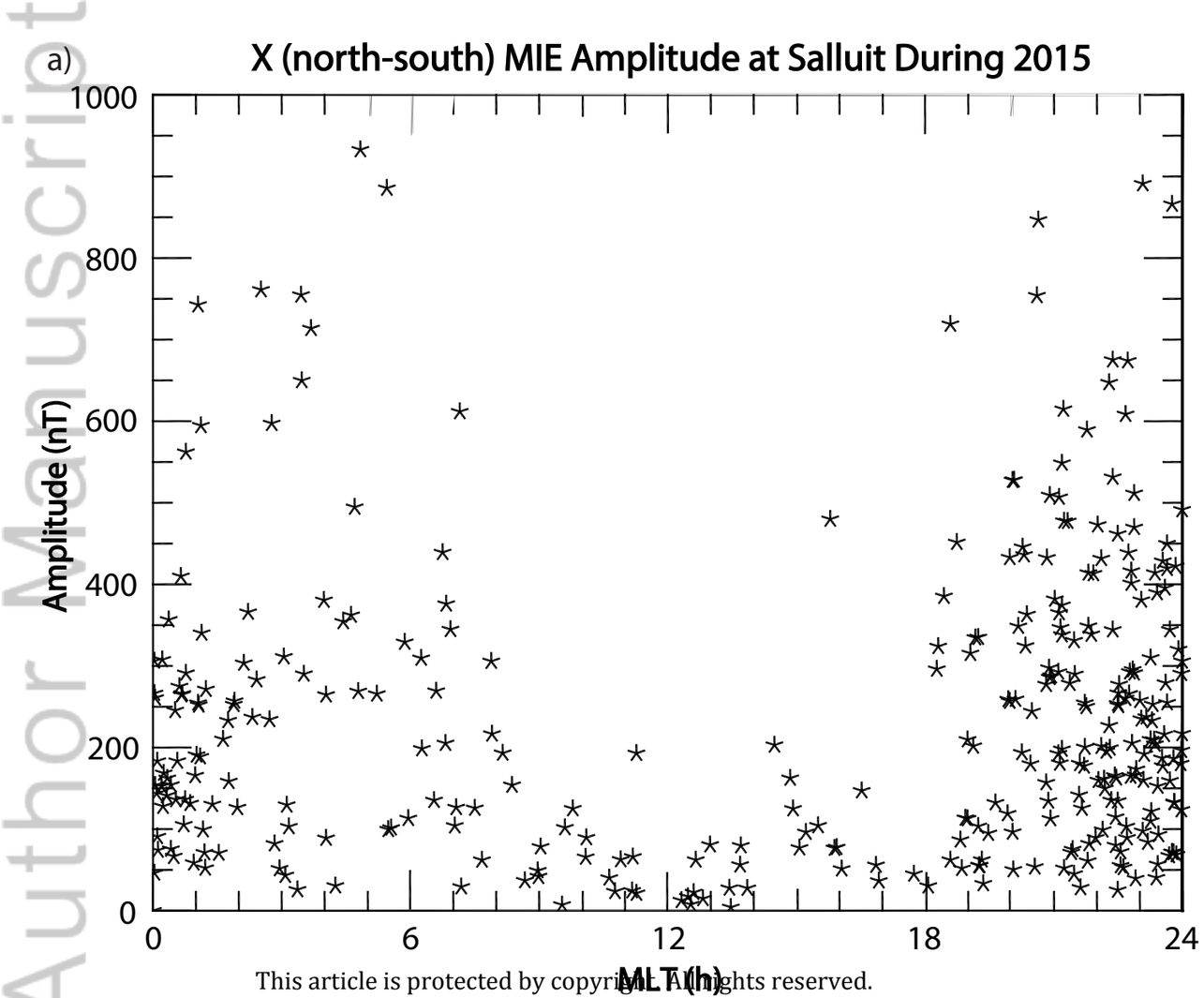

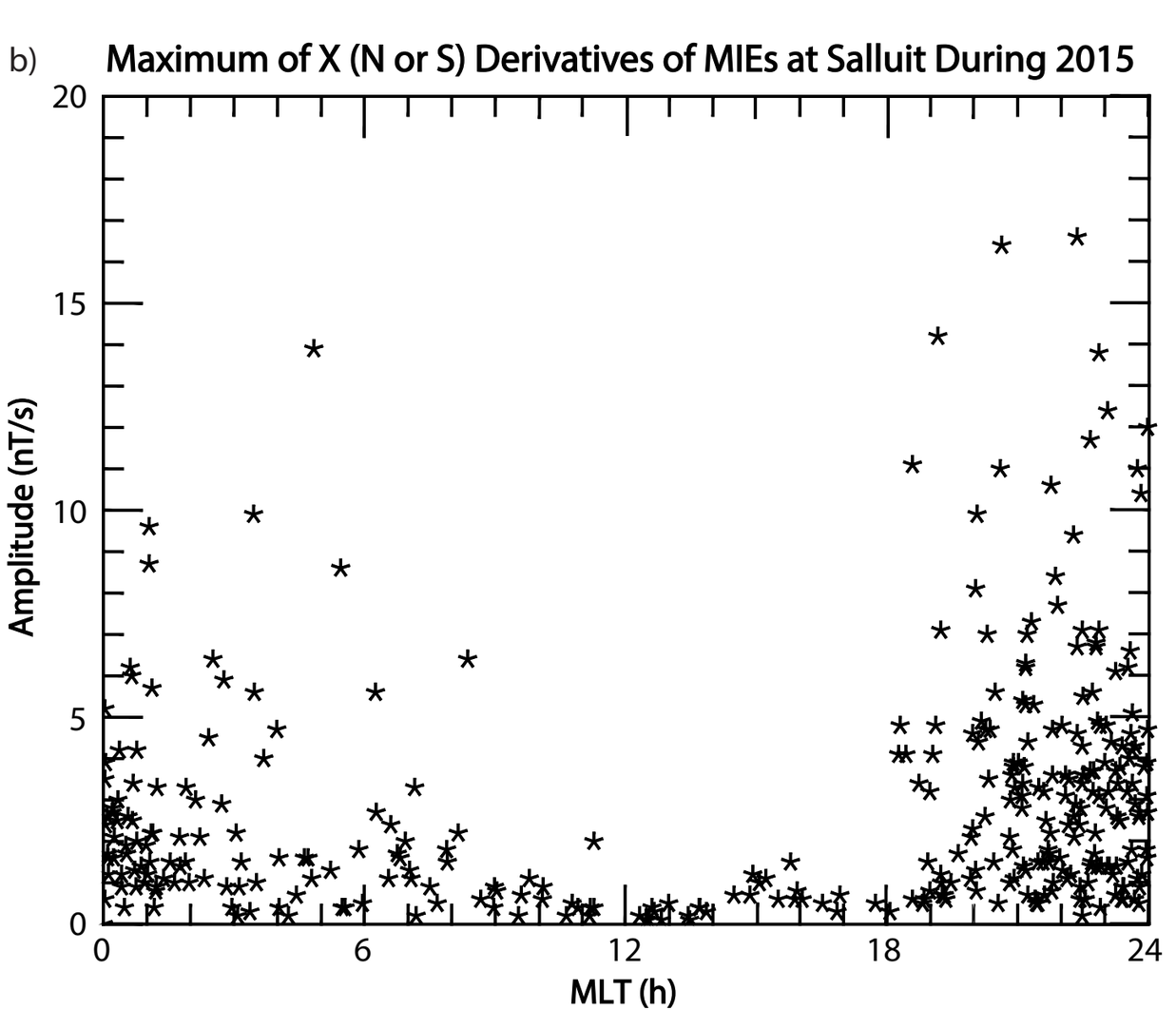

Extreme Magnetic Perturbation Events Observed During 2015 in Eastern and Central Arctic Canada

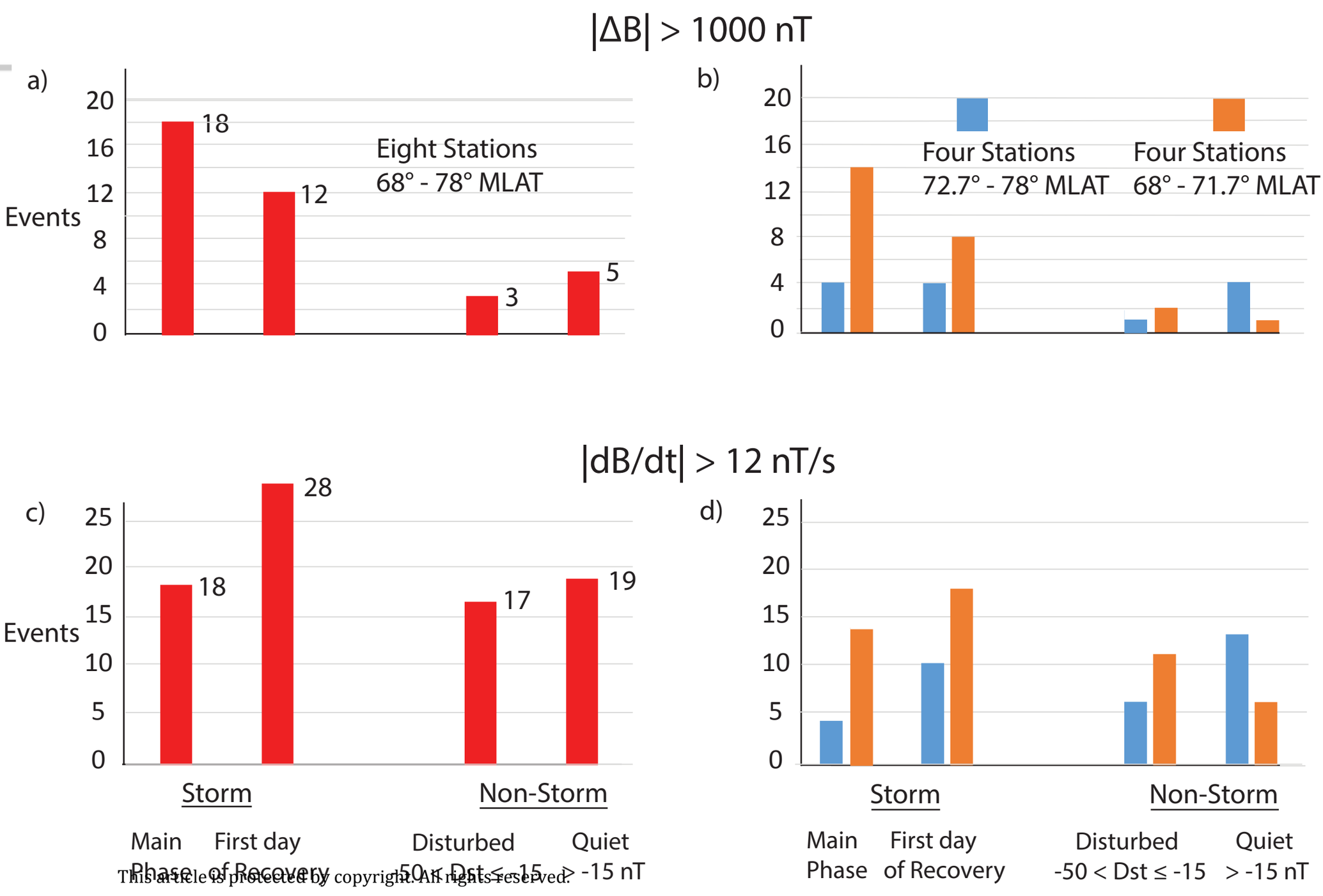

Time Delays from Substorm Onset until large dB/dt Occurrence